JVST B
Journal of Vacuum Science & Technology B

Atomic spectroscopy and laser frequency stabilization with scalable micrometer and sub-micrometer vapor cells

Cite as: J. Vac. Sci. Technol. B **38**, 050601 (2020); https://doi.org/10.1116/6.0000416
Submitted: 03 August 2020 . Accepted: 05 August 2020 . Published Online: 26 August 2020

Eliran Talker, Roy Zektzer, Yefim Barash, Noa Mazurski, and Uriel Levy

JVST B
Journal of Vacuum Science & Technology B

LETTER

avs.scitation.org/journal/jvb

Atomic spectroscopy and laser frequency stabilization with scalable micrometer and sub-micrometer vapor cells

Cite as: J. Vac. Sci. Technol. B 38, 050601 (2020); doi: 10.1116/6.0000416
Submitted: 3 August 2020 · Accepted: 5 August 2020 ·
Published Online: 26 August 2020

Eliran Talker, Roy Zektzer, Yefim Barash, Noa Mazurski, and Uriel Levy[a)]

AFFILIATIONS

Department of Applied Physics, The Benin School of Engineering and Computer Science, The Center for Nanoscience and Nanotechnology, The Hebrew University of Jerusalem, Jerusalem 91904, Israel

[a)]**Author to whom correspondence should be addressed:** ulevy@mail.huji.ac.il

ABSTRACT

We report on the atomic spectroscopy and laser frequency stabilization using a new type of a miniaturized glass vapor cell with a scalable thickness varying from 500 nm up to 8 μm. The cell is fabricated by lithography and etching techniques in a Pyrex glass substrate, followed by anodic bonding. It is filled with rubidium vapor using a distillation procedure. This simple and cost-effective fabrication method provides an attractive and compact solution for atomic cells, with applications in quantum metrology, sensing, communication, and light-vapor manipulations at the subwavelength scale. Using the fabricated cell, we have performed fluorescence and transmission spectroscopy of the Rubidium D2 line and observed sub-Doppler broadened lines. As an example, for a potential application, we have used the fabricated cell to demonstrate the stabilization of a 780 nm diode laser to the level about 10^{-10} in fractional frequency.

I. INTRODUCTION

The spectroscopy of atoms confined in miniaturized scale vapor cells[1–3] is a rapidly emerging field, with implications spanning from fundamentals such as precision analysis of atomic structures and atom-wall surface interactions[4–6] to applications such as atomic clocks[7–9] magnetometry,[10] and optical isolation.[11,12] One of the outcomes of using miniaturized cells is the increase in atom-surface interactions. This triggered the development of a new glass submicrometer and even nanometric (nm) scale cells.[13–17] Typically, the submicrometer and nm cells are made of two sapphire substrates with a titanium spacer in between serving as a space variant gap between the two sapphire substrates, making it a wedge-type structure. The two sapphire substrates are glued together. The cell is then evacuated and the alkali vapor is inserted into the cell using known distillation procedures. One of the drawbacks with such an approach is that the wedgelike structure prevents the two sapphire plates from being parallel to each other. Furthermore, the ability to customize the interior of the cell for specific needs is missing. Finally, atoms move across regions of different thicknesses, making the measurements of accurate thickness dependent phenomena more challenging. Hereby, we demonstrate a different method to design and fabricate a miniaturized vapor cell. The fabrication of our vapor cell is based on lithography and etching techniques, offering high parallelism and precise control over the shape and thickness of the vapor cell. We first describe the cell fabrication process and how it is filled with rubidium (Rb) alkali vapor. Subsequently, we present the measured fluorescent spectroscopy extracted from the cell for three different values of thickness and discuss the results. Finally, as an example for the usefulness of our concept, we use the cell to stabilize a diode laser down to the level of $\Delta f/f = 1 \times 10^{-10}$.

II. EXPERIMENT

A. Cell fabrication

Our cell consists of two glass wafers that are bonded together using the anodic bonding technique.[18] The first glass wafer is patterned to contain the desired cell geometry, as shown in Fig. 1. First, a 250 nm amorphous silicon (a-Si) layer is deposited on a Borofloat 33 glass wafer [50.8 mm diameter and a thickness of 1.3 mm, Fig. 1(a)] by plasma enhanced chemical vapor deposition

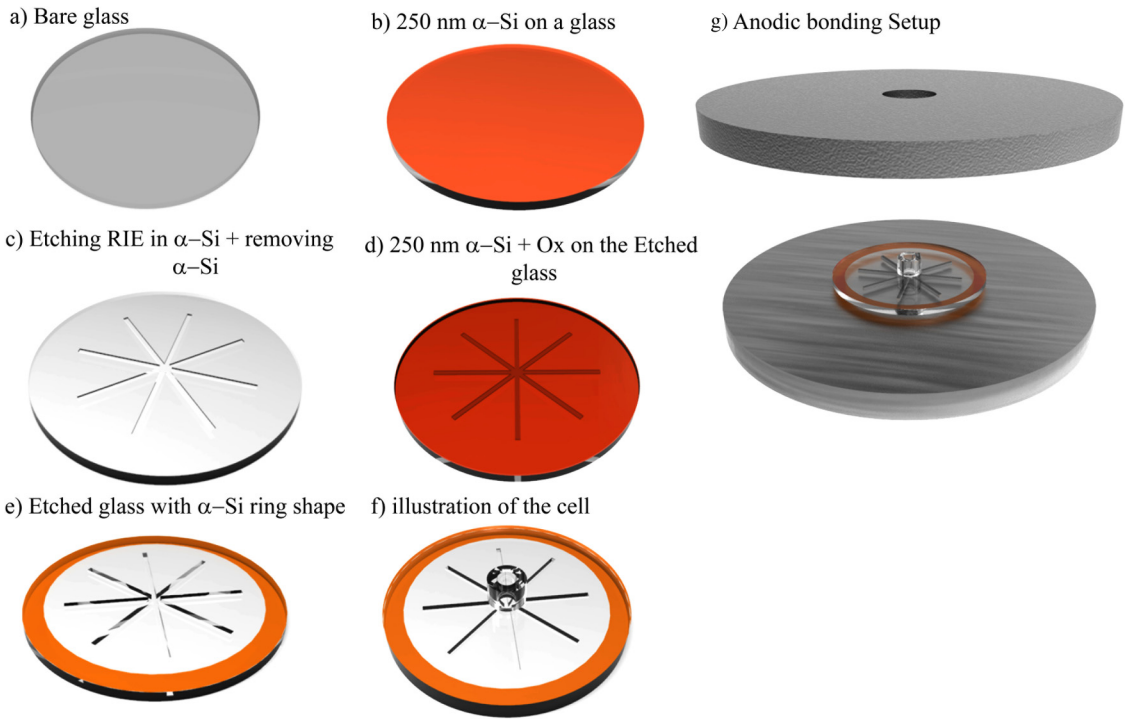

FIG. 1. Illustration of the fabrication process of the patterned glass substrate. The device consists of three channels with a common crossing point. Each of the three channel is etched to a different thickness (8, 5, and 0.5 μm), and they all are having a width of 1 mm and a length of 40 mm.

(PECVD) [Fig. 1(b)]. The glass wafer is spin-coated with HMDS (Hexamethyldisilazane, for a better adhesion) followed by a photoresist (PR) and baked for 2 min on a 110 °C hot plate [Fig. 1(b)]. The PR is exposed using a direct laser writing lithography system (UV 405 nm) and developed in a PR developer removing the exposed areas, thus defining the chamber geometry. Before etching, the glass is placed on a 135 °C hot plate for 45 min. Then, the a-Si layer is etched by reactive ion etching followed by wet etching of the glass in an HF:H_2O 1:10 solution. The typical etch rate is ~6 μm/h. After glass etching [see Fig. 1(c)], the PR was stripped in an acetone and isopropyl alcohol (IPA) followed by a "piranha" solution (also known as piranha etch, by a mixture of sulfuric acid H_2SO_4, water, and hydrogen peroxide H_2O_2) [Fig. 1(c)]. Then, the a-Si layer is removed by a KOH solution. The process is repeated three times, in order to create a device with three different chambers having different thickness (8, 5, and 0.5 μm). The result of a miniaturized vapor cell [Fig. 1(d)], consisting of three channels oriented at 120° with respect to each other with a common crossing point. Each channel is 40 mm long and 1 mm wide. Next, a new layer of 250 nm a-Si is deposited for the purpose of facilitating the process of anodic bonding to the other wafer, as described later in the text. Next, a layer of ~250 nm PECVD SiO_2, to be used as a hard mask for the consequent a-Si etching process, is deposited on top of the a-Si layer [Fig. 1(e)]. The glass wafer is then spin-coated with a PR and baked for 2 min on a 110 °C hot plate. Again, a laser writer is used to pattern the PR with the purpose of defining the shape of the a-Si layer to be used for the bonding purpose. Care is taken to make sure the a-Si layer resides outside of the channels. After 2 min baking on a 120 °C hot plate, the oxide layer was etched in a buffered oxide etch solution. Then, the PR is stripped in an acetone and IPA followed by a "piranha" solution. After rinsing in de-ionized water, a-Si was etched in the KOH solution, and the PECVD SiO_2 layer is removed in the buffered oxide etch solution [Fig. 1(f)]. By the end of this process, the glass wafer is ready for anodic bonding.

In parallel, another 1 cm thick, 2 in. diameter glass substrate is prepared in the following way. First, a through hole of about 4 mm in diameter is drilled. Next, the substrate is machined such that it is thinned down to about 2 mm thickness, besides the central part, effectively generating a short glass tube that will later allow be used to fill the cell. High quality polishing is applied to the glass, with surface roughness lower than 1.2 nm. Next, a longer glass tube is connected to the short tube using the glass blowing technique. The length of the first tube is fairly large (~1 cm long), and therefore the flame is far away from the plate and has a negligible influence its flatness. The processed substrate is shown in Fig. 1(f). The two glass substrates are now ready to be bonded together.

For the anodic bonding, we use the above-mentioned patterned glass wafer (substrate 1) and another substrate (substrate 2) containing a stem which is used for connecting the cell into a

vacuum chamber for the purpose of filling the cell with rubidium (Rb) vapor. The two substrates are stacked between two stainless steel electrodes. Between the stainless steel and each of the two substrates, we place a graphite plate in order to absorb the sodium ions and avoid damage to the glass. The whole stack is homogeneously heated to the bonding temperature of 350 °C. When the stack is at thermal equilibrium, a high voltage (700 V) is applied for 40 min, with the positive electrode connected to the lower glass substrate, and anodic bonding is achieved [Fig. 1(g)]. Following the anodic bonding process, the cell is baked out for 48 h using a turbo vacuum system, which is connected to the cell until a vacuum level in the range of 10^{-7}–10^{-8} Torr is reached. Finally, a droplet of natural Rb is inserted into the cell. The droplet is prepared by the condensation of Rb vapor in a vacuum system, which is connected to an alumino-silicate glass ampule containing rubidium chloride (RbCl) and calcium (Ca), placed in a high temperature furnace. The Rb vapor is obtained by reduction of the RbCl with Ca.[11] The reduction took place at an elevated temperature, producing gaseous Rb, which condensates on the cool surface of the glass system's main tube. Then, it transferred by a torch to the cell attached to the main tube, after which the cell was disconnected from the vacuum system and sealed.

B. Cell characterization

To perform optical characterization, the cell is enclosed in a homemade oven with small apertures to allow the laser beam to propagate through the cell and to provide the option of collecting the fluorescence light perpendicular to the laser beam. With this setup, we acquire the fluorescence spectra shown in Figs. 2(a)–2(c), alongside with the spectrum of a reference cell. These fluorescent spectra were obtained by scanning the frequency of a laser diode around the D2 line of Rb at the wavelength around 780 nm. In practice, one should pay attention to maintain the temperature of the cell at a higher temperature as compared to the cold spot in order to avoid condensation of Rb. The spectra of Fig. 2 were obtained for different values of cell thickness at a temperature of 150 °C (temperature of the reservoir, i.e., the cold spot), corresponding to a density of $\sim 3 \times 10^{13}$ (cm^{-3}) and thus to an effective number of atoms of 4.6×10^{10}, 2.9×10^{10}, and 2.9×10^{9} for the 8, 5, and 0.5 μm thickness, respectively. The outer line in panels (a)–(c) of Fig. 2 corresponds to the fluorescence signal from the reference cell, which was heated to 70 °C. This combination of high temperature and long cell dictates a relatively high optical density. As a result, the Rb85 and Rb87 hyperfine levels have almost the same contrast. During the measurements, the laser power was set to ~20 μW, and the laser spot at $1/e^2$ radius was 2 mm. In all cases, the measured fluorescence exhibits a line shape, which is narrower than the Doppler broadened line shape of a standard reference cell (7.5 cm long cell). Moreover, for the thinnest cell (0.5 μm), the linewidth is sufficiently narrow such that it is possible to identify the onset of hyperfine separation. We attributed this characteristic to the Dicke narrowing effect that has been observed in nanocells.[19] However, other reasons such as velocity-dependent collisions with the wall may also play a role. In order to verify that the Dicke effect is playing a role, we have calculated the area under each allowed transition and compared it to the number density. We have assumed a relaxation rate of ~9 MHz, which accounts for pressure broadening of the natural linewidth. For a 0.5 μm thick cell, the number density extracted from the measured curve is $\sim 10^{13}$(cm^{-3}) while the expected number density at 150 °C is $\sim 3 \times 10^{13}$(cm^{-3}) . Thus, the narrowing effect should be attributed, at least partially, to

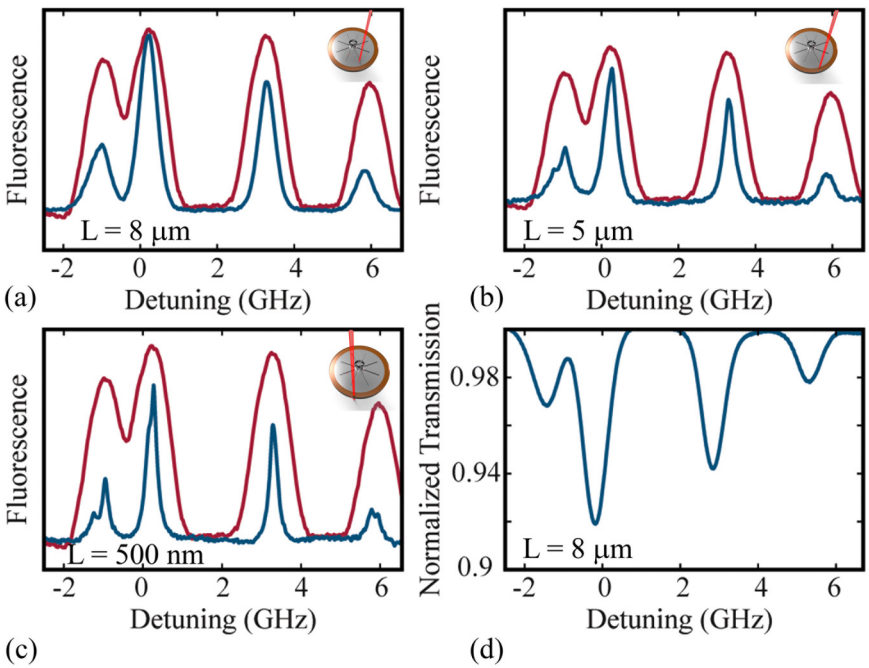

FIG. 2. (a)–(c) Comparison of fluorescence signal for the D2 transition as a function of frequency detuning from a reference cell (70 °C, the outer line) and the thin cell of three different values of thickness (150 °C, the inner line). (d) Transmission spectroscopy of the D2 transition measured in the 8 μm thick channel at 150 °C as a function of frequency detuning.

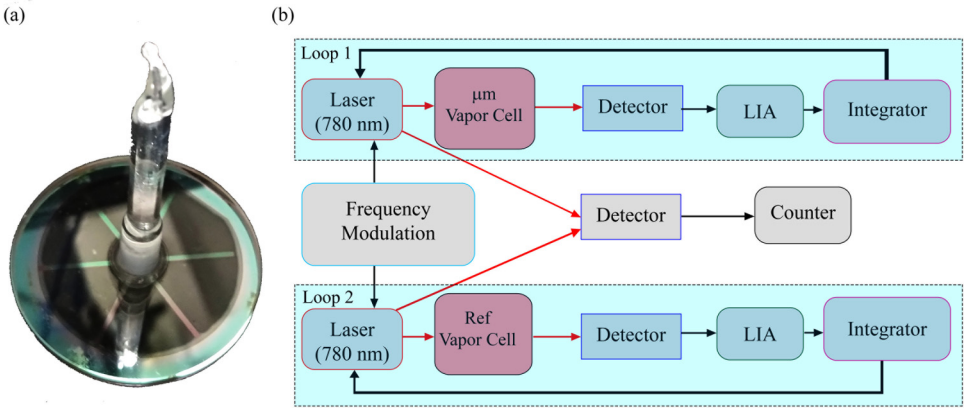

FIG. 3. (a) Photograph of the fabricated cell. (b) Frequency stabilization scheme. Two feedback loops are presented. The upper loop represents a 780-laser locked to our micrometer scale cell. The lower loop represents a 780 nm laser locked to rubidium reference cell (7.5 cm long).

collisions with the walls. This raises the following question: Do we still have contribution from Dicke narrowing? To address this question, we have also measured the area under the peak for the larger cells (5 and 8 μm thick) and found the number density to be even lower. And yet, the measured linewidth is larger. We believe that this indicates the onset of the Dicke narrowing effect in the thinnest (0.5 μm) cell. However, to study this effect in more detail, we will conduct a future experiment in which several cells with thickness in the wavelength and the subwavelength scale will be fabricated and characterized.

In Fig. 2(d), we show the transmission spectroscopy extracted from the 8-μm thick channel.

C. Laser frequency stabilization

To demonstrate the usefulness of obtaining a narrow linewidth, we use our miniaturized device to stabilize the frequency of a diode laser to the D2 line of Rb. The stabilization setup is shown in Fig. 3.

The locking scheme is presented in Fig. 3(b), where one tunable laser at 780 nm wavelength is locked by a wavelength modulation scheme to an absorption line of an Rb reference cell and the other laser is locked to the absorption line of our micrometer scale Rb cell. We have measured the beat signal between the two lasers and extracted the instability by Allan deviation. For comparison, we

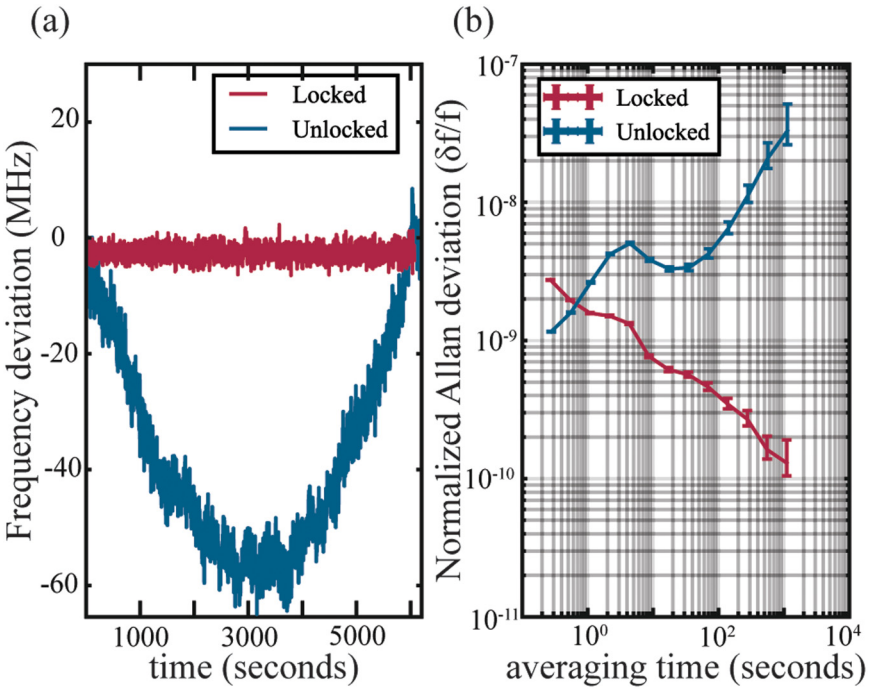

FIG. 4. (a) Measured beat frequency between two locked lasers (straight line) and between a locked laser to a free running laser (curved line) over a period of 6000 s. (b) Allan deviation of the beat signal obtained from the two locked (negative slope) lasers. The Allan deviation obtained from the locked laser and a free running laser is shown in positive slope.

have also measured the beat signal between a laser locked to a reference cell and a free running laser. Figure 4(a) shows the frequency difference between laser locked to a reference cell and the laser locked to our miniaturized cell as a function of time (red line). For comparison, we also display the frequency difference between laser locked to a reference cell and a free running laser as a function of time. The reference laser was locked to the level of $\sim 10^{-10}$ at 100 s, and it was positioned in a different room on a different table minimizing the effect of common noise rejection. One can clearly observe the improved stability obtained by locking the laser to our miniaturized cell. The Allan deviation results are depicted in Fig. 4(b), where the Allan deviation, which is the square root of the overlapping Allan variance, is shown.[20] The Allan deviation was calculated with a confidence factor of 0.683. The result shows laser stabilization down to the level of about 10^{-10} at 1000 s ($1.58 \times 10^{-9}/\tau^{0.5}$). Clearly, this result is significantly better than the stability of our free running laser, which has a frequency drift larger than 60 MHz/h [Fig. 4(a)], and it is only slightly worse than laser locked to the reference cell. Rb is a known frequency reference and lasers have been locked to it with instabilities better by two and even three orders of magnitude as compared to our results.[21,22] Yet, these results have been achieved with much larger vapor cells. If we consider a figure of merit defined as the system size multiplied by the instability, our obtained result is comparable and even superior to the results obtained with larger cells. We have measured the instability for several times on a couple of days and found a long-term shift in the frequency of a few MHzs. We attribute this relatively large shift to the effect of Fabry–Pérot interference fringes. These fringes are the result of reflection from the oven facets and are not a fundamental limitation of our micrometer scale device. As such, it can be improved in future versions.

III. CONCLUSIONS

To conclude, we have demonstrated atomic spectroscopy and laser frequency referencing using a new type of miniaturized and scalable vapor cell. The cell is manufactured in house using lithography and etching techniques, followed by anodic bonding. Using fluorescent spectroscopy, we observed sub-Doppler linewidth, and in the extreme case of the 0.5-μm thick channel, lines were sufficiently narrow to observe the hyperfine splitting. This is attributed to the effect of Dicke narrowing. Finally, we have used the vapor cell to stabilize the frequency of a diode laser to a stable atomic reference with accuracy of $\Delta f/f \sim 1 \times 10^{-10}$. This simple and cost-effective fabrication method provides an attractive and compact solution for atomic cells, with applications in metrology, sensing, communication, and light-vapor manipulations at the subwavelength scale.

ACKNOWLEDGMENTS

The research in this Letter was supported by the Israeli Science Foundation (ISF). E.T. acknowledges a fellowship from the Hebrew University Center for Nanoscience and Nanotechnology.

DATA AVAILABILITY

The data that support the findings of this study are available within the article.

REFERENCES

[1]J. Kitching, Appl. Phys. Rev. **5**, 031302 (2018).
[2]T. Baluktsian, C. Urban, T. Bublat, H. Giessen, R. Löw, and T. Pfau, Opt. Lett. **35**, 1950 (2010).
[3]W. Yang, D. B. Conkey, B. Wu, D. Yin, A. R. Hawkins, and H. Schmidt, Nat. Photonics **1**, 331 (2007).
[4]J. Keaveney, A. Sargsyan, U. Krohn, I. G. Hughes, D. Sarkisyan, and C. S. Adams, Phys. Rev. Lett. **108**, 173601 (2012).
[5]T. Peyrot, Y. R. P. Sortais, A. Browaeys, A. Sargsyan, D. Sarkisyan, J. Keaveney, I. G. Hughes, and C. S. Adams, Phys. Rev. Lett. **120**, 243401 (2018).
[6]K. A. Whittaker, J. Keaveney, I. G. Hughes, A. Sargsyan, D. Sarkisyan, and C. S. Adams, Phys. Rev. Lett. **112**, 253201 (2014).
[7]S. Knappe, P. D. D. Schwindt, V. Gerginov, V. Shah, L. Liew, J. Moreland, H. G. Robinson, L. Hollberg, and J. Kitching, J. Opt. A Pure Appl. Opt. **8**, S318 (2006).
[8]F. Benabid, F. Couny, J. C. Knight, T. A. Birks, and P. S. J. Russell, Nature **434**, 488 (2005).
[9]K. Fukuda, M. Kinoshita, A. Hasegawa, M. Tachikawa, and M. Hosokawa, J. Natl. Inst. Inf. Commun. Technol. **50**, 95 (2003).
[10]P. D. D. Schwindt, S. Knappe, V. Shah, L. Hollberg, J. Kitching, L. A. Liew, and J. Moreland, Appl. Phys. Lett. **85**, 6409 (2004).
[11]E. Talker, P. Arora, M. Dikopoltsev, and U. Levy, J. Phys. B **53**, 045201 (2020).
[12]L. Weller, K. S. Kleinbach, M. A. Zentile, S. Knappe, I. G. Hughes, and C. S. Adams, Opt. Lett. **37**, 3405 (2012).
[13]B. Zambon and G. Nienhuis, Opt. Commun. **143**, 308 (1997).
[14]A. Mikata, U. Tanaka, and S. Urabe, Appl. Opt. **47**, 639 (2008).
[15]S. Briaudeau, D. Bloch, and M. Ducloy, Europhys. Lett. **35**, 337 (1996).
[16]C. Andreeva, S. Cartaleva, L. Petrov, S. M. Saltiel, D. Sarkisyan, T. Varzhapetyan, D. Bloch, and M. Ducloy, Phys. Rev. A **76**, 1 (2007).
[17]T. F. Cutler, W. J. Hamlyn, J. Renger, K. A. Whittaker, D. Pizzey, I. G. Hughes, V. Sandoghdar, and C. S. Adams, e-print arXiv: 2004.10577 (2020).
[18]A. Berthold, L. Nicola, P. M. Sarro, and M. J. Vellekoop, Sens. Actuators A **82**, 224 (2000).
[19]D. Sarkisyan, T. Varzhapetyan, A. Sarkisyan, Y. Malakyan, A. Papoyan, A. Lezama, D. Bloch, and M. Ducloy, Phys. Rev. A **69**, 065802 (2004).
[20]W. J. Riley, *Handbook of Frequency Stability Analysis* (NIST, Boulder, Colorado, 2008).
[21]L. Stern *et al.*, Sci. Adv. **6**, eaax6230 (2020).
[22]M. T. Hummon *et al.*, Optica **5**, 443 (2018).